Break-up of shells under explosion and impact

F. K. Wittel[1], F. Kun[2*], H. J. Herrmann[3], and B. H. Kröplin[1]

[1]*Institute of Statics and Dynamics of Aerospace Structures,*
University of Stuttgart, Pfaffenwaldring 27, 70569 Stuttgart, Germany
[2]*Department of Theoretical Physics, University of Debrecen, P. O. Box:5, H-4010 Debrecen, Hungary*
[3]*ICP, University of Stuttgart, Pfaffenwaldring 27, D-70569 Stuttgart, Germany*
(Dated: February 2, 2008)

A theoretical and experimental study of the fragmentation of closed thin shells made of a disordered brittle material is presented. Experiments were performed on brown and white hen egg-shells under two different loading conditions: fragmentation due to an impact with a hard wall and explosion by a combustion mixture giving rise to power law fragment size distributions. For the theoretical investigations a three-dimensional discrete element model of shells is constructed. Molecular dynamics simulations of the two loading cases resulted in power law fragment mass distributions in satisfactory agreement with experiments. Based on large scale simulations we give evidence that power law distributions arise due to an underlying phase transition which proved to be abrupt and continuous for explosion and impact, respectively. Our results demonstrate that the fragmentation of closed shells defines a universality class different from that of two- and three-dimensional bulk systems.

PACS numbers: 64.60.-i, 64.60.Ak, 46.30.Nz

Closed shells made of solid materials are often used in every day life, industrial applications and engineering practice as containers, pressure vessels or combustion chambers. From a structural point of view aircraft vehicles, launch vehicles like rockets and building blocks of a space station are also shell-like systems, and even certain types of modern buildings can be considered as shells. The egg-shell as nature's oldest container proved to be a reliable construction for protecting life. In most of the applications shell-like constructions operate under an internal pressure much higher than the surrounding one. Hence, careful design and optimization of structural and material properties is required to ensure the stability and reliability of the system. Closed shells usually fail due to an excess internal load which can arise either as a result of slowly driving the system above its stability limit during its usage or service time, or by a pressure pulse caused by an explosive shock inside the shell. Due to the widespread applications, the failure of shell systems is a very important scientific and technological problem which has also an enormous social impact due to the human costs arising, for instance, in accidental events.

Fragmentation, *i.e.* the breaking of particulate materials into smaller pieces is abundant in nature and underlies several industrial processes, which attracted a continuous interest in scientific and engineering research over the past decades [1, 2, 3, 4, 5, 6, 7, 8, 9, 10, 11, 12, 13, 14, 15, 16]. Fragmentation phenomena can be observed on a broad range of length scales ranging from the collisional evolution of asteroids and meteor impacts on the astrophysical scale, through geological phenomena and industrial applications on the intermediate scale down to the break-up of large molecules and heavy nuclei on the atomic scale. In laboratory experiments on the fragmentation of solids, the energy input is usually achieved by shooting a projectile into a solid block [4, 5, 6, 7, 8, 9], making an explosion inside the sample [2, 3] or by the collision of macroscopic bodies (free fall impact) [11, 12, 13, 14, 15, 16]. Due to the violent nature of the process, observations on fragmenting systems are often restricted to the final state, making the fragment size (volume, mass, charge, ...) to be the main characteristic quantity. The most striking observation on fragmentation is that the distribution of fragment sizes shows a power law behavior, independently on the way of imparting energy, relevant microscopic interactions and length scales involved, with an exponent depending only on the dimensionality of the system [2, 3, 4, 5, 6, 7, 8, 9, 10, 11, 12, 13, 14, 15, 16, 17]. During the past years experimental [2, 3, 4, 5, 6, 7, 8, 9, 10, 11, 12, 13, 14, 15, 16, 17] and theoretical [18, 19, 20, 21, 22, 23, 24, 25, 26, 27, 28, 29, 30, 31, 32, 33, 34, 35, 36, 37, 38, 39, 40, 41] efforts focused on the validity region and the reason of the observed universality in 1, 2, and 3 dimensions. Detailed studies revealed that universality prevails for large enough input energies when the system falls apart into small enough pieces [7, 8, 9, 10, 13, 14, 15, 16, 18, 19, 20, 21, 22, 23, 24, 25, 26, 27], however, at lower energies a systematic dependence of the exponent on the input energy was evidenced [28, 29]. Recent investigations on the low energy limit of fragmentation suggest that the power law distribution of fragment sizes arises due to an underlying critical point [21, 22, 27, 34, 35, 38].

Besides the industrial and social impact of the failure of shell like systems, they are also of high scientific importance for the understanding of fragmentation phenomena. Former studies on fragmentation have focused on the behavior of bulk systems in one, two and three dimensions under impact and explosive loading, however,

hardly any studies have been devoted to fragmentation of shells [38]. The peculiarity of the break-up of closed shells originates from the fact that the local structure is inherently two-dimensional, however, the dynamics of the systems, the motion of material elements, deformation and stress states are three-dimensional which allows for a rich variety of failure modes [38].

In this paper we present a detailed experimental and theoretical study of the fragmentation of closed solid shells arising due to an excess load inside the shell. Experiments were performed on brown and white hen egg-shells under two different loading conditions: fragmentation due to an impact with a hard wall and explosion by a combustion mixture have been considered resulting in power law fragment size distributions. For simplicity, our theoretical study is restricted to spherical shells such that a three dimensional discrete element model of spherical shell systems was worked out. In molecular dynamics simulations of the two loading cases, power law fragment mass distributions were obtained in satisfactory agreement with experiments. Based on large scale simulations we give evidence that power law distributions arise due to an underlying phase transition which proved to be abrupt for explosion and continuous for impact. Analyzing the energetics of the explosion process in the two loading cases and the evolution of the fragment mass distributions we demonstrate that the fragmentation of closed shells defines a new universality class different from that of two- and three-dimensional bulk systems.

I. EXPERIMENTS

Hen eggs provide an excellent possibility for the study of fragmentation of thin brittle shells of disordered materials with the additional advantages of being cheap and easy to handle, making the patience of scientists the only limiting factor for the subsequent improvement of the experimental results. Our experiments were performed on ordinary brown and white egg-shells. In the preparations, first two holes of regular circular shape were drilled on the bottom and top of the egg through which the content of the egg was blown-out. The inside was carefully washed and rinsed out several times and finally the empty shells were dried in a microwave oven to get rid of all moisture of the egg-shell. The drying process proved to be essential to ensure that the cuticula, which cannot be blown out, competely looses its toughness.

In the impact experiments intact egg-shells are catapulted onto the ground at a high speed using a simple setup of rubber bands. The experimental setup provided a relatively high energy impact without the possibility of varying the imparted energy. The eggs are shot directly into a plastic bag touching the ground so that no fragments are lost for further evaluation.

In the explosion experiment initially the egg-shell is flooded with hydrogen and hung vertically inside a plastic bag. The combustion reaction is initiated by igniting the
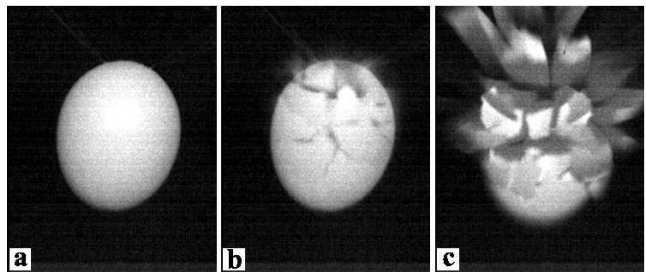

FIG. 1: Time evolution of the explosion of an egg-shell, consecutive snapshots taken by a high speed camera. The time difference between the snapshots is 0.001 sec.
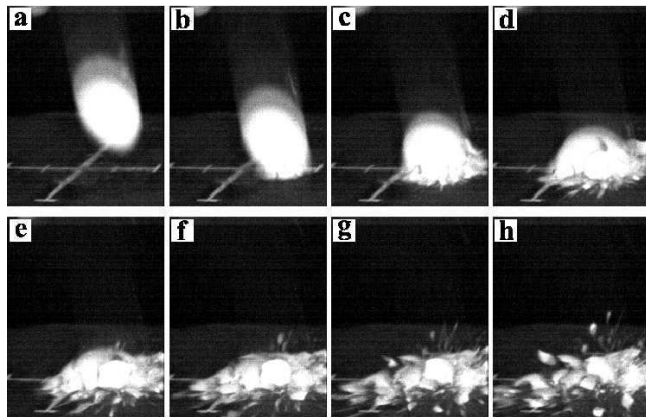

FIG. 2: Time series of the impact of an egg-shell with the hard ground. The consecutive snapshots were taken by a high speed camera of 1 kHz.

escaping hydrogen on the top of the egg. The hydrogen immediately reacts with the Oxygen which is also drawn up into the egg through the bottom hole, mixing with the remaining hydrogen. When enough air has entered to form a combustible mixture inside the egg, the flame back-fires through the top hole and starts the very quick exothermic reaction. The experiment is carried out inside a soft plastic bag so that secondary fragmentations due to fragment-wall collisions do not occur, furthermore, no pieces were lost after explosion. Since the pressure which builds up during combustion can slightly be changed by the hole size, *i.e* the smaller the hole, the higher the pressure at the explosion, we performed several series of experiments with hole diameters d between 1.2 and 2.5 millimeter. The limit values have practical reasons: a drilling nail of large diameter typically breaks the eggs-shell, on the other hand it is extremely difficult to blow out an egg through a hole of diameter 1 mm or less.

It is possible to follow the time evolution of the explosion and impact processes by means of a high speed camera under well controlled conditions. Three consecutive snapshots of the explosion process are presented in Fig. 1 taken by a camera of 1000 Hz frequency. The ignition took place at the top of the egg in Fig. 1a). The
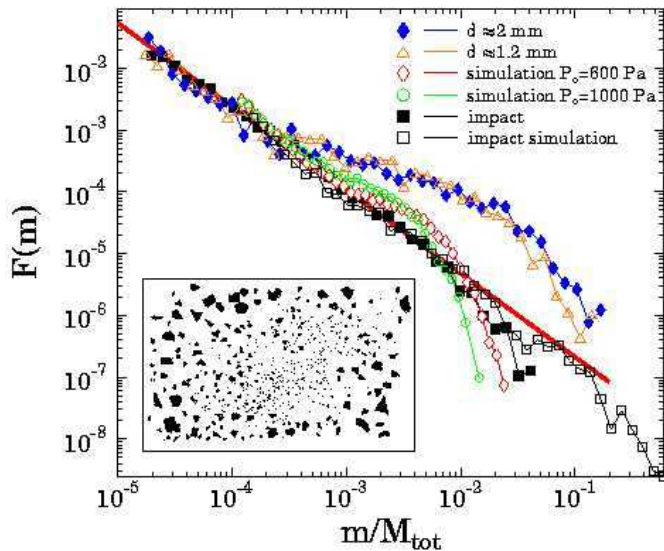
FIG. 3: Comparison of fragment mass distributions obtained by explosion experiments with two hole sizes and the impact experiment to the simulation results. The inset shows a typical scanned set of fragments.

instant of back-firing and the initiation of combustion is captured in Fig. 1b), while in Fig. 1c) already the flying pieces can be seen. Based on the snapshots the total duration of an explosion is estimated to be of the order of 1 millisecond.

In the impact experiment the egg hits the ground in the direction of its longer axis, as it is illustrated by the picture series of Fig. 2. After hitting the ground (Fig. 2b), the egg suffers gradual collapse as it moves forward (Fig. 2c − h) making the impact process relatively longer compared to the explosion.

The resulted egg-shell pieces are then carefully collected and placed on the tray of a scanner without overlap. In the scanned image fragments are seen as black spots on a white background and were further analyzed by a cluster searching code. In the inset of Fig. 3 an example of scanned pieces of an impact experiment is shown where the broad variation of sizes can also be noticed with the naked eye. A dusty phase of shattered pieces [42] was also observed in the experiments with fragment sizes falling in the order of the pixel size of the scanner. The mass m of fragments was determined as the number of pixels in the scanned image. Since shattered fragments were also comparable to normal dust pieces in the air, they were excluded in the analysis by setting the lower cut-off of fragment masses to a few pixels.

As the main quantitative result of the experiments we evaluated the mass distribution of fragments $F(m)$ which is defined so that $F(m)\Delta m$ provides the probability of finding a fragment with mass falling between m and $m+\Delta m$. Fig. 3 presents the fragment mass distribu-

tions $F(m)$ for impact and explosion experiments averaged over 10-20 egg-shells for each curve. For the impact experiment, a power law behavior of the fragment mass distribution

$$F(m) \sim m^{-\tau} \tag{1}$$

can be observed over three orders of magnitude where the value of the exponent can be determined with high precision to $\tau = 1.35 \pm 0.02$. Explosion experiments result also in a power law distribution of the same value of τ for small fragments with a relatively broad cut-off for the large ones. Smaller hole diameter d in Fig. 3, *i.e.* higher pressure, gives rise to a larger number of fragments with a smaller cut-off mass and a faster decay of the distribution $F(m)$ at the large fragments. Comparing the number of fragments obtained, the ratio of the pressure values in the explosions at hole diameters $d = 1.2$ and 2.0 mm, presented in Fig. 3, was estimated to be about 1.6. Note that the relatively small value of the exponent τ can indicate a cleavage mechanism of shell fragmentation and is significantly different from the experimental and theoretical results on fragmenting two-dimensional bulk systems where $1.5 \leq \tau \leq 2$ has been found [2, 7, 8, 13, 14, 15, 16, 21, 22, 34, 35, 36, 37], and from the three-dimensional ones where $\tau > 2$ is obtained [2, 5, 6, 39, 40].

II. SIMULATIONS

Most of the theoretical studies on fragmentation relay on large scale computer simulations since capabilities of analytic approaches are rather limited in this field due to the complexity of the break-up process. Over the past years the Discrete Element Method (DEM) proved to be a very efficient numerical technique for fragmentation phenomena [21, 22, 27, 34, 35, 36, 37, 38, 39, 40, 41] since it has the ability to handle large deformations arising dynamically, and naturally captures the propagation and interaction of a large number of simultaneously growing cracks, which is essential for fragmentation.

In order to investigate the fragmentation of spherical shells we constructed a three-dimensional discrete element model such that the surface of the unit sphere is discretized into randomly shaped triangles (Delaunay triangulation) by throwing points randomly and independently on the surface [43, 44]. Based on the triangulation, the dual Voronoi tessellation of the surface is also carried out as is illustrated in Fig. 4. The nodes of the triangulation represent point-like material elements in the model whose mass is defined by the area of the Voronoi polygon assigned to it [36, 43, 44]. The bonds between nodes are assumed to be springs having linear elastic behavior up to failure. Disorder is introduced in the model solely by the randomness of the tessellation so that the mass assigned to the nodes, the length and cross-section of the springs are determined by the tessellation (quenched structural disorder). After prescribing the initial conditions of a specific fragmentation process, the time evolution of the
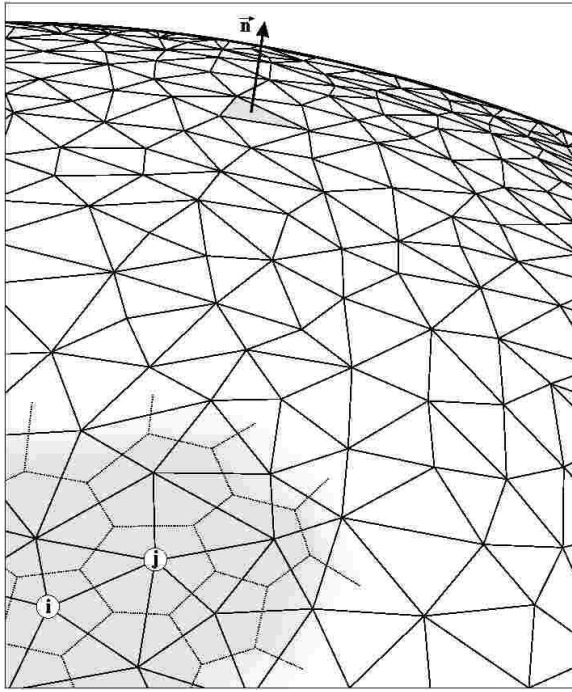
FIG. 4: Example of the Delaunay triangulation of the spherical surface. The dual Voronoi lattice is also shown in the lower left quadrant.

Parameter	Symbol	Unit	Value
Initial radius	R	m	1
Initial volume	V_o	m^3	4.19
Initial Surface	A_o	m^2	12.56
Shell thickness	th	m	$5 \cdot 10^{-5}$
Total mass	M_{tot}	kg	0.816
Num. of triangles	N_t		≈ 44000
Num. of nodes	N_n		≈ 21000
Mass density	ρ	kg/m^3	1300
Time step	Δt	s	$3 \cdot 10^{-7}$
Damping coeff.	γ_d	kg/s	0.1
Spring Young modul.	Y	N/m^2	10^9

TABLE I: Parameter values used in the simulations.

accessible experimentally, providing a deep insight into the fragmentation process. With the present computer capacities, DEM models can be designed to be realistic so that the simulation results can even complement the experimental information extending our understanding. The most important parameter values used in our simulations are summarized in Table I.

In computer simulations two different ways of loading have been considered which model the experimental conditions and represent limiting cases of energy input rates: (i) *pressure pulse* and (ii) *impact* load. A pressure pulse in a shell is carried out by imposing a fixed internal pressure P_o from which the forces $\vec{F}_j^{ext}$ acting on the triangular surface elements are calculated as

$$\vec{F}_j^{ext} = P_o A_j \vec{n}_j, \qquad (3)$$

where A_j denotes the actual area of triangle j and the force points in the direction of the local normal $\vec{n}_j$, see also Fig. 4. The force F_j^{ext} is equally shared by the three nodes of the triangle for which the equation of motion Eq. (2) is solved. Since the surface area of the shell increases, the expansion under constant pressure implies a continuous increase of the driving force and of the imparted energy.

The impact loading realizes the limiting case of instantaneous energy input by giving a fixed initial radially oriented velocity v_o to the material elements and following the resulted time evolution of the system by solving the equation of motion Eq. (2). The control parameter of the system which determines the final outcome of the process are the fixed pressure P_o and the initial kinetic energy E_o for the pressure pulse and impact loading, respectively.

III. THE BREAK-UP PROCESS

In the simulations, in both loading cases the spherical shell is initially completely stress free with no energy stored in deformation. When a constant pressure is imposed the total energy E_{tot} of the shell increases due to
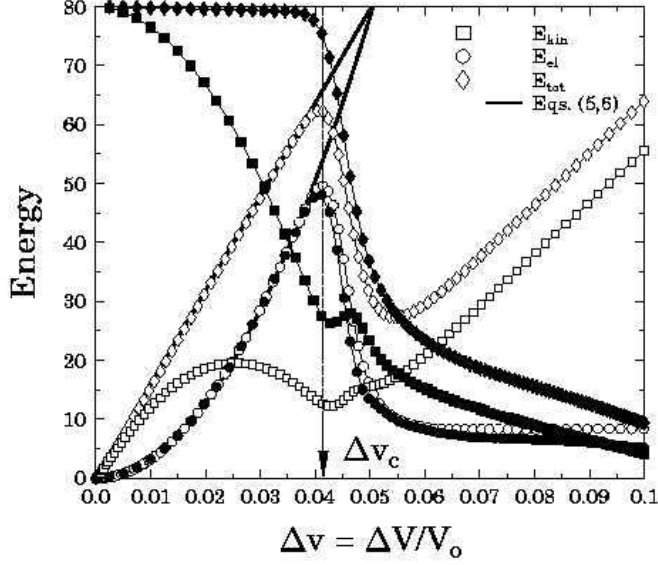
system is followed by solving the equation of motion of nodes by a Predictor-Corrector method of fourth order

$$m_i \ddot{\vec{r}}_i = \vec{F}_i^s + \vec{F}_i^{ext} + \vec{F}_i^d, \quad i = 1, \dots N, \qquad (2)$$

where $\vec{F}_i^s$ is the sum of forces exerted by the springs connected to node i, and $\vec{F}_i^{ext}$ denotes the external driving force, which depends on the loading condition. To facilitate the relaxation of the system at the end of the fragmentation process, a small viscous damping force $\vec{F}_i^d$ was also introduced in Eq. (2).

In order to account for crack formation in the model springs are assumed to break when their deformation ε exceeds a certain breaking threshold ε_c. A fixed threshold value $\varepsilon_c = 0.03$ is set for all the springs resulting in a random sequence of breakings due to the disordered spring properties. The breaking criterion is evaluated at each iteration step and those springs which fulfill the condition are removed from the simulation. As a result of successive spring breakings cracks nucleate, grow and merge on the spherical surface which can give rise to a complete break-up of the shell into smaller pieces.

Fragments of the shell are defined in the model as sets of nodes (material elements) connected by the remaining intact springs. The process is stopped when the system has attained a relaxed state, *i.e.* when there is no spring breaking over a large number of iteration steps. The main advantage of DEM is that it makes it possible to monitor a large number of microscopic physical quantities during the course of the simulation which are hardly

FIG. 5: The kinetic E_{kin}, elastic E_{el}, and total E_{tot} energies as a function of the relative volume change Δv. Open symbols stand for expansion under constant pressure while the filled ones characterize the impact loading. The sudden drop of the total and elastic energy at Δv_c indicates the rapid break-up of the system. For E_{tot} of the pressure loading the thick solid line follows Eq. (5), while for E_{el} the function given by Eq. (6) was fitted with $C = 312000$ as a parameter.

FIG. 6: Cracks on the shell surface. Final states of impact experiments at energies $E_o/E_c \approx 0.8$ $a)$ and 2.8 $b)$. Time evolution of the cracking process under a constant pressure of $P_o/P_c \approx 4.0$ $c,d)$ until the final relaxed state is reached $e)$, with a magnified view of fragments $f)$. Particle positions are projected back to their initial state on the surface. Fragments are identified as shell pieces surrounded by cracks.

the work done by the filling gas

$$E_{tot}(V) = \int_{V_o}^{V} P_o dV = P_o \Delta V, \qquad (4)$$

where V denotes the actual volume during the expansion and ΔV is the volume change with respect to the initial state V_o. The total energy can be written as the sum of the kinetic energy of material elements E_{kin} and of the elastic energy E_{el} stored in deformation, $E_{tot} = E_{kin} + E_{el}$, where E_{el} is proportional to the change ΔA of surface area A of the expanding sphere with respect to the initial surface A_o. Introducing the relative volume change $\Delta v = \frac{\Delta V}{V_o}$ as an independent variable, the total energy and the elastic energy can be cast in the form

$$E_{tot} = P_o V_o \Delta v, \qquad (5)$$

$$E_{el} = C \left[(\Delta v + 1)^{1/3} - 1 \right]^2, \qquad (6)$$

where the surface change ΔA was expressed in terms of Δv. Furthermore, the parameter C of the system depends on the properties of the triangulation and the characteristic physical quantities of springs (Young modulus, length, thickness). It is interesting to note that there exists a specific pressure value P_o^* below which the expansion always stops at a maximum volume change
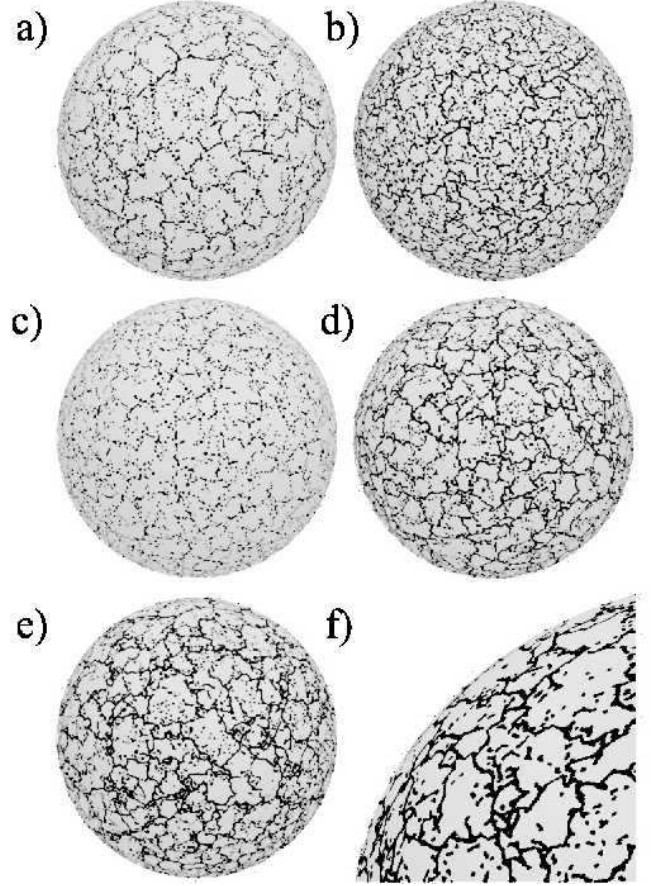
Δv_{max} depending on P_o, however, for $P_o > P_o^*$ the expansion keeps always accelerating. For a given $P_o < P_o^*$ the value of Δv_{max} can be determined from the condition $E_{tot} = E_{el}$ so that

$$P_o V_o \Delta v_{max} = C \left[(\Delta v_{max} + 1)^{1/3} - 1 \right]^2, \qquad (7)$$

and P_o^* can be identified as the highest pressure for which Eq. (7) can be solved for Δv_{max}. Usually Δv_{max} can only be realized at low pressure values, because at higher pressures the system suffers complete break-up much below Δv_{max}, due to the finite strength of the springs. Fig. 5 illustrates the evolution of the total E_{tot}, kinetic E_{kin}, and elastic E_{el} energies as a function of Δv for both pressure and impact loading. In the case of pressure loading it can be observed that the total energy E_{tot} extracted from the simulations agrees well with the analytic prediction of Eq. (5). The numerical value of the multiplication factor C of the elastic energy was obtained by fitting the

expression Eq. (6) to the curve of $E_{el}(\Delta v)$ in the figure. Due to the constant pressure, the total force F acting on the shell is proportional to the actual surface area $F \sim A \cdot P_o$ so that the system is driven by an increasing force during the expansion process. Since the driving force F increases with a diminishing rate when approaching the limit volume change Δv_{max}, it follows that the pressure loading case is analogous to the stress controlled quasistatic loading of bulk specimens. According to the simulations, under pressure loading there exists a critical pressure P_c below which the expansion always stops at a finite volume and the shell only suffers partial failure *(damage)* in the form of cracks but it keeps its integrity. When the pressure exceeds P_c, however, the system surpasses the critical volume change Δv_c when abruptly a large amount of springs break resulting in the break-up of the system *(fragmentation)*. Note that $P_c << P_o^*$.

The critical volume change Δv_c where fragmentation sets in during the expansion can be identified by the location of the sudden drop of the elastic energy in Fig. 5 caused by the large amount of spring breaking which occurs in a very narrow Δv interval, resulting in a rapid formation of cracks on the surface. The value of Δv_c is mainly determined by the fixed breaking threshold ε_c and the disordered spring properties. Since the shell is under constant pressure the nucleated microcracks can grow and join giving rise to planar pieces surrounded by a free crack surface (fragment), as is illustrated in Fig. 6c, d, e. First large fragments are formed which then break-up into smaller pieces until the surviving springs can sustain the remaining stress, see Fig. 6c, d, e. For simplicity, in the simulations the pressure is kept constant even if the system has lost its integrity, which has formally the consequence that pieces of the shell formed in the final state of fragmentation keep accelerating under the action of a constant force which explains the increasing kinetic energy E_{kin} in Fig. 5 following fragmentation. The volume of the system is numerically calculated as the sum of the volume of pyramidal objects defined by the surface elements and the center of the sphere, which provides a meaningful result even after break-up in Fig. 5 in the vicinity of Δv_c. The critical pressure P_c, required to exceed the critical volume change Δv_c to achieve fragmentation, can be estimated as $P_c = E_{el}(\Delta v_c)/(V_o \Delta v_c)$.

When loading is imposed by an instantaneous energy input E_o, there is no further energy supply, the total energy of the system is either constant or decreases due to the viscous dissipation and the breaking of springs (see Fig. 5). Since the elastic energy E_{el} is solely determined by the deformation, the curve of E_{el} and the critical volume change Δv_c where break-up arises in Fig. 5 coincide with the corresponding values of the pressure loading. Similarly to the pressure loading case, simulations revealed that a critical value of the imparted energy E_c can be identified below which the shell maintains its integrity suffering only damage, while exceeding E_c gives rise to a complete fragmentation of the shell. The resulted fragments on the shell surface obtained in the fragmented

regime can be seen in Fig. 6a, b).

IV. FRAGMENT MASSES

To give a quantitative characterization of the break-up of shells and to reveal the nature of the transition between the damaged and fragmented states large scale simulations have been performed varying the control parameters, *i.e.* the fixed pressure P_o, and the imparted energy E_o over a broad range. The most important characteristics of our fragmenting shell system, that can be compared to the experimental findings is the variation of fragment masses when changing the control parameters. In the simulations two cut-offs arise for the fragment masses, where the lower one is defined by the single unbreakable material elements of the model and the upper one is due to the finite size of the system.

For both types of loading above the critical point the typical fragment size obtained at the instant of break-up decreases with increasing control parameter, which can be described analytically in terms of an energy balance argument similarly to the one given in Ref. [26]. The loading energy of a shell region of linear extension L and mass $m \sim L^2$, *i.e.* the energy stored in the motion of particles separating the piece from its surrounding, can be written as $[m/M_{tot}] E_{kin}(\Delta v_c)L^2 = [E_{kin}(\Delta v_c)/M_{tot}] L^4$, where $E_{kin}(\Delta v_c)$ denotes the total kinetic energy of the shell at the instant of break-up and M_{tot} is the total mass of the shell. The separation of the piece from its surrounding costs energy proportional to the fragment surface $\sim L$. The equilibrium fragment size can be obtained by minimizing the sum of the loading and surface energy densities ρ_E

$$\rho_E \sim \frac{E_{kin}(\Delta v_c)}{M_{tot}}L^2 + \frac{1}{L}, \qquad (8)$$

with respect to L, which results in $L \sim E_{kin}^{-1/3}$. It has been shown in the previous section that at the critical point P_c, E_c the total kinetic energy of the system when break-up occurs takes zero value $E_{kin}(\Delta v_c) = 0$. It follows that above the critical point E_{kin} has a linear dependence on the distance from the critical point so that $E_{kin}(\Delta v_c) \sim (P_o - P_c)$ for $P_o > P_c$, and $E_{kin}(\Delta v_c) \sim (E_o - E_c)$ for $E_o > E_c$ hold. Substituting these results into Eq. (8), the typical fragment mass at the instant of break-up can be cast into the form

$$m \sim (P_o - P_c)^{-2/3} \quad \text{for} \quad P_o > P_c, \qquad (9)$$
$$m \sim (E_o - E_c)^{-2/3} \quad \text{for} \quad E_o > E_c. \qquad (10)$$

Eqs. (9,10) express that the typical fragment mass obtained at the time of break-up decreases according to a power law with increasing distance from the critical point. The exponent of the power law is universal in the sense that it does not depend on specific material properties of the shell. Later on during the fragmentation
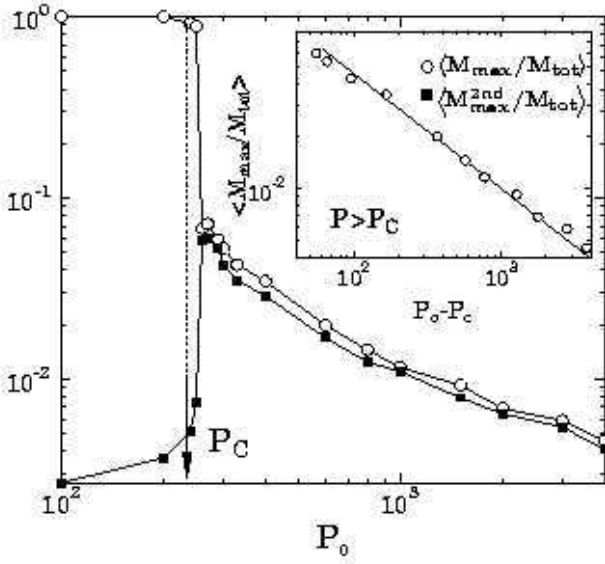
FIG. 7: Average mass of the largest $\langle M_{max}/M_{tot}\rangle$ and second largest $\langle M_{max}^{2nd}/M_{tot}\rangle$ fragment normalized by the total mass as a function of imposed pressure P_o. The inset presents a log-log plot of $\langle M_{max}/M_{tot}\rangle$ as a function of the distance from the critical point $P_o - P_c$. In the main figure the value of P_c is indicated by an arrow.

FIG. 8: $\langle M_{max}/M_{tot}\rangle$ and $\langle M_{max}^{2nd}/M_{tot}\rangle$ as a function of the imparted energy. The inset presents a log-log plot of the largest mass as a function of $|E_o - E_c|$, where the increasing and decreasing branches characterize the damaged and fragmented states, respectively. The location of E_c is indicated in the main figure.

process the elastic energy stored in deformation may result in succesive breakings of the large fragments. Hence, it can be expected that Eqs. (9,10) describe the scaling behaviour of the largest fragments, which did not undergo substantial size reduction until reaching the final relaxed state.

Largest fragments. To characterize the degree of fragmentation, *i.e.* the size reduction achieved in the simulations, we calculated the average mass of the largest $\langle M_{max}/M_{tot}\rangle$ and of the second largest $\langle M_{max}^{2nd}/M_{tot}\rangle$ fragment normalized by the total mass as a function of the pressure P_o, and input energy E_o in the case of pressure and impact loading, respectively [34, 35]. The results are presented in Figs. 7, and 8. It can be seen that in both cases the maximum fragment mass is a monotonically decreasing function of the control parameters P_o and E_o, however, the functional forms are different in the two cases. Low pressure values in Fig. 7 result in a breaking of springs, however, hardly any fragments are formed except for single elements broken out of the shell along cracks. Hence, the mass of the largest fragment is practically equal to the total mass M_{tot} of the system, while the second largest fragment is orders of magnitude smaller (*damage*). Increasing however the pressure above the threshold value P_c the largest fragment mass becomes much smaller than the total mass, furthermore, in this regime there is only a slight difference between the largest and second largest fragments, indicating the complete disintegration of the shell into pieces (*fragmentation*). The value of the critical pressure
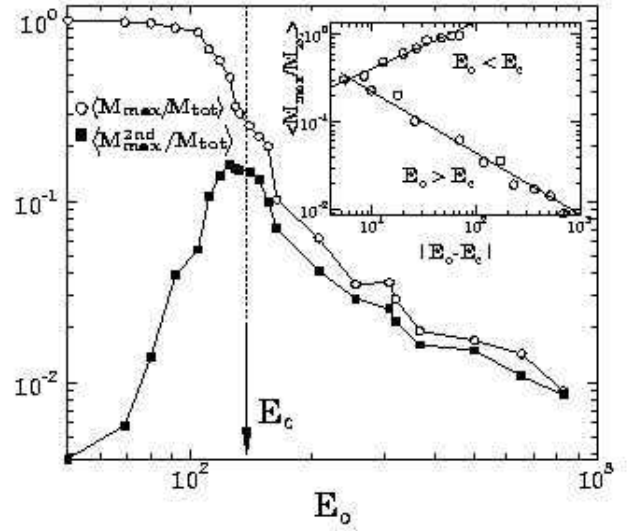
P_c needed to achieve fragmentation and the functional form of the curve of $\langle M_{max}/M_{tot}\rangle$ above P_c was determined such that $\langle M_{max}/M_{tot}\rangle$ was plotted as a function of the difference $|P_o - P_c|$ varying P_c until a straight line is obtained on a double logarithmic plot. The result is presented in the inset of Fig. 7 where a power law dependence of $\langle M_{max}/M_{tot}\rangle$ is evidenced as a function of the distance from the critical point

$$\langle M_{max}/M_{tot}\rangle \sim |P_o - P_c|^{-\alpha}, \quad \text{for} \quad P_o > P_c. \quad (11)$$

The exponent $\alpha = 0.66\pm0.02$ was obtained in good agreement with the analytic prediction of Eq. (9). Detailed studies in the vicinity of P_c revealed a finite jump of both $\langle M_{max}/M_{tot}\rangle$ and $\langle M_{max}^{2nd}/M_{tot}\rangle$ at P_c which implies that fragmentation occurs as an abrupt transition at the critical point, see Fig. 7.

In Fig. 8 the corresponding results are presented for the case of impact loading as a function of the total energy E_o imparted to the system initially. The mass of the largest fragment is again a monotonically decreasing function of the control parameter, however, it is continuous in the entire energy range considered. Careful analyzes revealed the existence of two regimes with a continuous transition at a critical value of the imparted energy E_c. In the inset of Fig. 8 $\langle M_{max}/M_{tot}\rangle$ is shown as a function of the distance from the critical point $|E_o - E_c|$ where E_c was determined using the same technique as for P_c. Contrary to the pressure loading, $\langle M_{max}/M_{tot}\rangle$ exhibits a power law behavior on both sides of the critical point but with
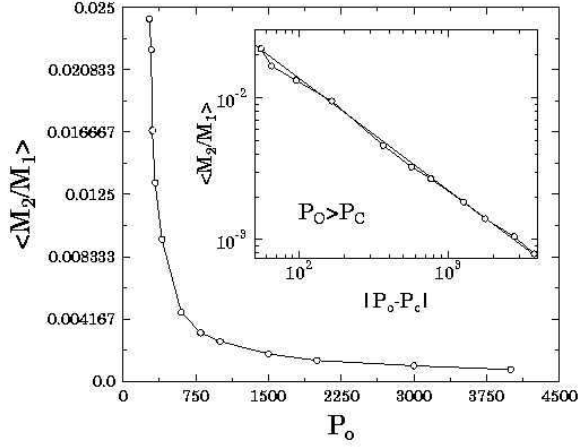
FIG. 9: The average fragment mass as a function of the imposed pressure P_o. The inset presents a log-log plot of the average mass as a function of the distance from the critical point $P_o - P_c$ for pressure values $P_o > P_c$. The value of P_c is the same as in Fig. 7.
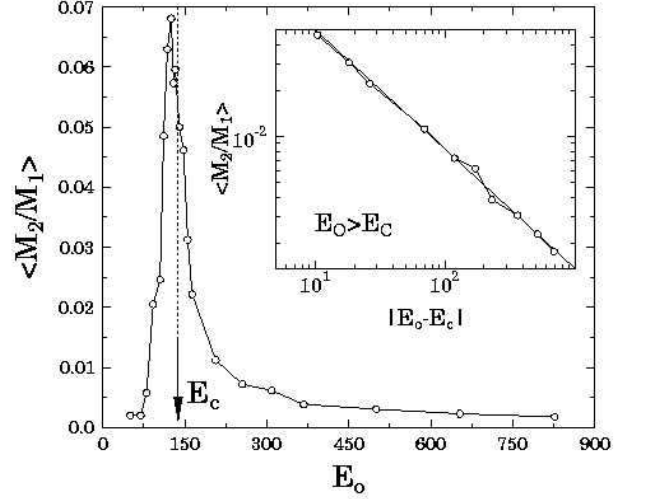

FIG. 10: The average fragment mass $\langle M_2/M_1 \rangle$ as a function of the imparted energy E_o. The two regimes can be clearly distinguished. The location of the critical point proved to be exactly the same as in Fig. 8. The inset shows a log-log plot of the average mass as a function of $|E_o - E_c|$.

different exponents

$$\langle M_{max}/M_{tot} \rangle \sim |E_o - E_c|^{\beta}, \quad \text{for} \quad E_o < E_c, \quad (12)$$
$$\langle M_{max}/M_{tot} \rangle \sim |E_o - E_c|^{-\alpha}, \text{ for} \quad E_o > E_c. \quad (13)$$

The numerical values of the exponents were obtained as $\alpha = 0.66 \pm 0.02$ and $\beta = 0.5 \pm 0.02$, above and below the critical point respectively. Note that the value of α coincides with the corresponding exponent of the pressure loading and is in a good agreement with the analytic prediction of Eq. (10). Below the critical point the second largest fragment is again orders of magnitude smaller than the largest one, which implies that in this energy range the shell suffers only damage in the form of cracks, while above the critical point the break-up of the entire shell results in comparable values of the largest and second largest fragment masses. At the transition point E_c between the damaged and fragmented states the mass of the second largest fragment has a maximum, while the curve of the largest one exhibits a curvature change, see Fig. 8.

Average fragment mass. More insight can be obtained into the fragmentation process by studying the so-called single-event moments of fragment masses

$$M_k^j = \sum_m m^k n^j(m) - M_{max}^k, \quad (14)$$

where M_k^j denotes the kth moment of fragment masses m in the jth realization of a fragmentation process, $n^j(m)$ is the number of fragments of mass m in event j. The ratio of the second M_2^j and the first M_1^j moments provides a measure for the average fragment mass in a specific

experiment j

$$\overline{M}^j = \frac{M_2^j}{M_1^j}. \quad (15)$$

Averaging over simulations with different realizations of disorder the average fragment mass $\overline{M} = \left\langle M_2^j/M_1^j \right\rangle$ was obtained as a function of the control parameter of the system.

Due to the abrupt nature of the transition from the damaged to the fragmented states at the critical pressure, under pressure loading $\overline{M}$ cannot be evaluated below P_c. However, when P_o exceeds the critical pressure P_c the average fragment mass monotonically decreases in Fig. 9. The inset of Fig. 9 shows $\overline{M}$ as a function of the distance from the critical point $|P_o - P_c|$ where the same value of P_c was used as in Fig. 7. A power law dependence of $\overline{M}$ is evidenced as a function of $|P_o - P_c|$

$$\overline{M} \sim |P_o - P_c|^{-\gamma}, \quad (16)$$

for $P_o > P_c$ and the value of the exponent was obtained to be $\gamma = 0.8 \pm 0.02$. For impact loading $\overline{M}$ can be evaluated on both sides of the critical point with a sharp peak in the vicinity of E_c which is typical for continuous phase transitions in finite systems, see Fig. 10. A power law dependence of $\overline{M}$ on the distance from the critical point

$$\overline{M} \sim |E_o - E_c|^{-\gamma} \quad (17)$$

is again revealed for $E_o > E_c$, which is illustrated in the inset of Fig. 10. The value of the exponent was determined by fitting $\gamma = 0.79 \pm 0.02$, which practically coincides with the γ value of pressure loading.
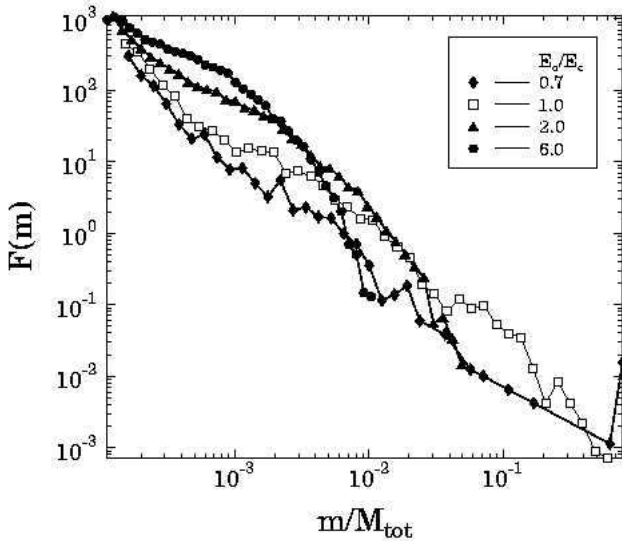
FIG. 11: Mass distribution of fragments at various energies below and above the critical point.

FIG. 12: Mass distribution of fragments at various pressure values.

Fragment mass distributions. The most important characteristic quantity of our system which can also be compared to the experimental results is the mass distribution of fragments $F(m)$. Under impact loading for $E_o < E_c$ we found that $F(m)$ has a pronounced peak at large fragments indicating the presence of large damaged pieces, see Fig. 11. Approaching the critical point E_c the peak gradually disappears and the distribution asymptotically becomes a power law at E_c. We can observe in Fig. 11 that above the critical point the power law remains for small fragments followed by a cut-off for the large ones, which decreases with increasing E_o.

For pressure loading $F(m)$ can only be evaluated above P_c. The evolution of $F(m)$ with increasing pressure is presented in Fig. 12, where the mass distribution always shows a power law behavior for small fragments with a relatively broad cut-off for the large ones. For the purpose of comparison, a mass distribution $F(m)$ obtained at an impact energy close to the critical point E_c, and distributions at two different pressure values P_o of the ratio 1.6 are plotted in Fig. 3 along with the experimental results. For impact an excellent agreement with the experimental and theoretical results is evidenced. For pressure loading, the functional form of $F(m)$ has a nice qualitative agreement with the experimental findings on the explosion of eggs, furthermore, distributions at the same ratio of pressure values obtained by simulations and experiments show the same tendency of evolution, see Fig. 3.

Figs. 13 and 14 demonstrate that by rescaling the mass distributions above the critical point by plotting $F(m) \cdot \overline{M}^\delta$ as a function of $m/\overline{M}$ an excellent data collapse is obtained with $\delta = 1.6 \pm 0.03$. The data collapse implies
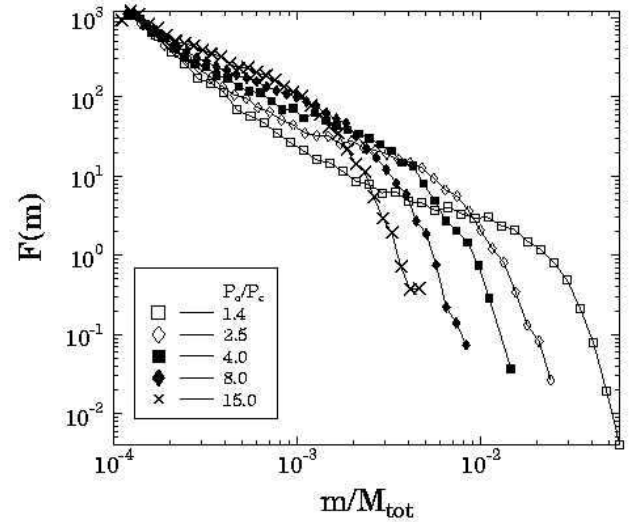
the validity of the scaling form

$$F(m) \sim m^{-\tau} \cdot f(m/\overline{M}), \qquad (18)$$

typical for critical phenomena. The cut-off function f has a simple exponential form $\exp\left(-m/\overline{M}\right)$ for impact loading (see Fig. 13), and a more complex one containing also an exponential component for the pressure case (see Fig. 14). The average fragment mass $\overline{M}$ occurring in the scaling form Eq. (18) diverges according to a power law given by Eqs. (16,17) when approaching the critical point. The good quality of collapse and the functional form Eq. (18) also imply that the exponent τ of the mass distribution does not depend on the value of the pressure P_o or the kinetic energy E_o contrary to the bulk fragmentation where an energy dependence of τ was reported [28].

The rescaled plots make possible an accurate determination of the exponent τ, where $\tau = 1.35 \pm 0.03$ and $\tau = 1.55 \pm 0.03$ were obtained for impact and pressure loading, respectively. Hence, a good quantitative agreement of the theoretical and experimental values of the exponent τ is evidenced for the impact loading of shells, however, for the case of pressure loading the numerically obtained exponent turned out to be somewhat higher than in the case of exploded eggs.

V.   DISCUSSION AND OUTLOOK

We presented a detailed experimental and theoretical study of the break-up of closed shells arising due to a shock inside the shell. For the purpose of experiments brown and white hen egg-shells were carefully prepared to ensure a high degree of brittleness of the disordered shell material. The break-up of the shell was studied under two different loading conditions, *i.e.* explosion
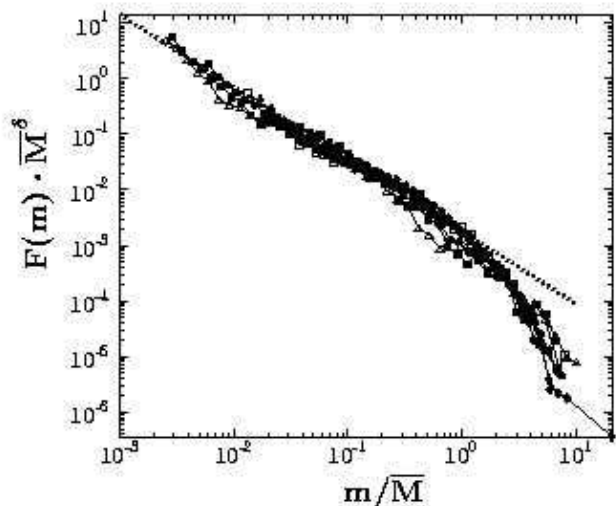
FIG. 13: Rescaled plot of the mass distributions for imparted energies above the critical point $E_o > E_c$. The dashed line shows the fitted power law with an exponent $\tau = 1.35 \pm 0.03$.

FIG. 14: Rescaled plot of the mass distributions of various pressure values above the critical point $P_o > P_c$. The dashed line indicates the fitted power law with an exponent $\tau = 1.55 \pm 0.03$.

caused by a combustible mixture and impact with the hard ground. As the main outcome of the experiments, the mass distribution of fragments proved to be a power law in both loading cases for small fragment sizes, however, qualitative differences were obtained in the limit of large fragments for the shape of the cut-off.

We worked out a discrete element model for the break-up of shells which provides an insight into the dynamics of the process by simultaneously monitoring several microscopic quantities in the framework of molecular dynamics simulations. In the simulations two ways of loading have been considered, which mimic the experimental conditions and represent limiting cases of energy input rates: during an expansion under constant pressure P_o the shell is driven by an increasing force with a continuous increase of the imparted energy, while the impact loading realizes the instantaneous input of an energy E_o. Simulations revealed that depending on the value of P_o and E_o, the final outcome of the break-up process can be classified into two states, *i.e.* damaged and fragmented with a sharp transition in between at a critical value of the control parameters P_c and E_c. In the fragmented regime power law fragment mass distributions were obtained in satisfactory agreement with the experimental findings. Analyzing the behavior of the system in the vicinity of the critical point P_c, E_c, we showed that power law distributions arise in the break-up of shells due to an underlying phase transition between the damaged and fragmented states, which proved to be abrupt for explosion, and continuous for impact.

Due to its unique characteristics, the break-up of shells defines a new universality class of fragmentation phenomena, different from that of the two- and three-dimensional bulk systems. 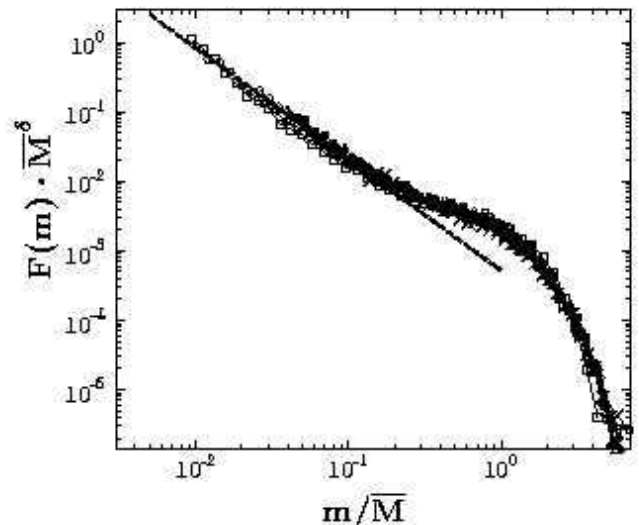Based on universality, our results should be applicable to describe the break-up of other closed shell systems composed of disordered brittle materials. Explosion of shell-like fuel containers, tanks, high pressure vessels often occur as accidental events in industry, or in space missions where also the explosion of complete satellites may occur creating a high amount of space debris orbiting about Earth. For the safety design of shell constructions, and for the tracking of space debris it is crucial to have a comprehensive understanding of the break-up of shells. Due to the universality of fragmentation phenomena, our results can be exploited for these purposes.

In the fragmentation of bulk systems under appropriate conditions a so-called detachment effect is observed when a surface layer breaks off from the bulk and undergoes a separated fragmentation process [28, 36]. This effect also shows up in the fragment mass distributions in the form of a power law regime of small fragments of an exponent smaller than for the large ones. Our results on shell fragmentation can also provide a possible explanation of this kind of composite power laws of bulk fragmentation [28, 36].

IKP.

[1] *Fragmentation Phenomena*, edited by D. Beysens, X. Campi, and E. Pefferkorn (World Scientific, 1995).

[2] D. L. Turcotte, J. of Geophys. Res. **91 B2**, 1921 (1986).

[3] L. Zhang, X. Jin, and H. He, J. Phys. D: Appl. Phys. **32** 612 (1999).

[4] J. J. Gilvarry, J. Appl. Phys. **32**, 391 (1961); J. Appl. Phys. **32**, 400 (1961).

[5] T. Matsui, T. Waza, K. Kani and S. Suzuki, J. of Geophys. Res. **87 B13**, 10968 (1982).

[6] A. Fujiwara and A. Tsukamoto, Icarus **44**, 142 (1980).

[7] H. Inaoka, E. Toyosawa, and H. Takayasu, Phys. Rev. Lett. **78**, 3455 (1997).

[8] T. Kadono, Phys. Rev. Lett. **78**, 1444 (1997).

[9] T. Kadono and M. Arakawa Phys. Rev. E **65**, 035107 (2002).

[10] H. Inaoka, M. Ohno, Fractals **11**, 369 (2003).

[11] F. G. Bridges, A. Hatzes, and D. N. C. Lin, Nature **309**, 333 (1984).

[12] N. Arbiter, C. C. Harris and G. A. Stamboltzis, Soc. of Min. Eng. **244**, 119 (1969).

[13] L. Oddershede, P. Dimon, and J. Bohr, Phys. Rev. Lett. **71**, 3107 (1993).

[14] A. Meibom and I. Balslev, Phys. Rev. Lett. **76**, 2492 (1996).

[15] H. Katsuragi, D. Sugino, and H. Honjo Phys. Rev. E **68**, 046105 (2003).

[16] H. Katsuragi, D. Sugino, H. Honjo, preprint cond-mat/0310479.

[17] X. Campi and H. Krivine, Z. Phys. A **344**, 81 (1992).

[18] S. Steacy and C. Sammis, Nature **353**, 250 (1991).

[19] H. Inaoka and H. Takayasu, Physica A **229**, 1 (1996).

[20] M. Marsili and Y. C. Zhang, Phys. Rev. Lett. **77**, 3577 (1996).

[21] J. Åström and J. Timonen, Phys. Rev. Lett. **78**, 3677 (1997).

[22] J. Åström, M. Kellomäki and J. Timonen, Phys. Rev. E **55**, 4757 (1997).

[23] R. Botet and M. Ploszajczak, Int. Jour. Mod. Phys. E **3**, 1033 (1994).

[24] R. Englman, J. Phys.: Condens. Matter **3**, 1019 (1991).

[25] G. Hernandez and H. J. Herrmann, Physica A **215**, 420 (1995).

[26] Wm. T. Ashurst and B. L. Holian, Phys. Rev. E **59**, 6742 (1999).

[27] J. A. Aström, B. L. Holian, and J. Timonen, Phys. Rev. Lett. **84**, 3061 (2000).

[28] E. S. C. Ching, S. Liu, and K. - Q. Xia, Physica A **287**, 83 (2000).

[29] A. Diehl, H. A. Carmona, L. E. Araripe, J. S. Andrade, Jr., and G. A. Farias, Phys. Rev. E **62**, 4742 (2000).

[30] A. Bershadskii, J. Phys. A **33**, 2179 (2000).

[31] A. Bershadskii, E. S. C. Ching, J. Stat. Phys. **104**, 49 (2001).

[32] A. Bershadskii, Chaos Solitons and Fractals **13**, 185 (2002).

[33] P. L. Krapivsky and E. Ben-Naim Phys. Rev. E **68**, 021102 (2003).

[34] F. Kun and H. J. Herrmann, Phys. Rev. E **59**, 2623 (1999).

[35] B. Behera, F. Kun, S. McNamara, and H. J. Herrmann, preprint cond-mat/0404057.

[36] F. Kun and H. J. Herrmann, Comput. Meth. Appl. Mech. Eng. **138**, 3 (1996).

[37] F. Kun and H. J. Herrmann, Int. Jour. Mod. Phys. C **7**, 837 (1996).

[38] F. Wittel, F. Kun, H. J. Herrmann, and B.-H. Kröplin, Physical Review Letters in print, cond-mat/0402461.

[39] C. Thornton, K. K. Yin and M. J. Adams, J. Phys. D Appl. Phys. **29**, 424 (1996).

[40] W. Benz and E. Asphaug, Icarus **107**, 98 (1994).

[41] A. V. Potapov, M. A. Hopkins and C. S. Campbell, Int. J. of Mod. Phys. **C 6**, 399 (1995).

[42] S. Redner, in *Statistical Models for the Fracture of Disordered Media*, edited by H. J. Herrmann and S. Roux (North Holland, Amsterdam, 1990).

[43] C. Moukarzel and H. J. Herrmann, J. Stat. Phys. **68**, 911 (1992).

[44] K. B. Lauritsen, H. Puhl and H. J. Tillemans, Int. J. Mod. Phys. C **5**, 909 (1994).